Photon detection efficiency of Geiger-mode avalanche photodiodes

S. Gentile[1], E. Kuznetsova[2], F. Meddi[1]

1- Università degli Studi di Roma "La Sapienza",
Piazzale Aldo Moro 5, 00185 Roma, Italy.

2- DESY,
Notkestraße 85, 22607, Hamburg, Germany.

The photon detection efficiencies of multi-pixel Geiger-mode avalanche photodiodes manufactured by different producers are estimated. A new fit method of the response spectra to low-intensity light, taking into account after-pulse and cross-talk effects is proposed to yield the initial number of photons. The value of photon detection efficiency is calculated using a calibrated photodetector as a reference.

1 Introduction

Multi-pixel Geiger-mode avalanche photodiodes (G-APDs) are solid-state photodetectors based on a technology developed since early 1990's [1, 2, 3, 4, 5, 6, 7, 8, 9]. Their gain is typically 10^6 per photoelectron. Their main features are: the small size, the efficiency comparable to the one of vacuum photomultipliers, the insensitivity to magnetic field, a low bias voltage and a reasonable price. Currently, the G-APDs find an application in many fields of physics, High-Energy, Neutrino, Astroparticle and Medicine.

This paper describes the results of a comparative study performed in the same experimental conditions, on different G-APDs, to allow an optimal choice with a view to a given application. We refer to elsewhere for a complete description of measurements and analysis methods [10].

2 General principle of the G-APD operation and its characteristics

A G-APD consists of a large number of identical microcells (silicon diodes, pixels) with a common anode. The microcells are located on a common substrate with a typical size of $\sim 1 \times 1$ mm^2. Once photoelectron are produced an electron avalanche multiplication may occur under a reverse bias, V_{bias}, above the breakdown voltage, V_{brd} and the charge induced during the avalanche discharge is proportional to the overvoltage ($V_{over} = V_{bias} - V_{brd}$). The number of fired pixels is proportional to the initial number of photoelectrons, as long as this is on average less than one per pixel. This implies a low-intensity light source in the measurement setup. The gain (g) is determined by the charge released in one pixel.

Other characteristics of the G-APD response to light deserve a few words.

After-Pulses (AP) appear when the quenching (mechanism to stop the avalanche process by temporally reducing the cell voltage) doesn't drain all the charge in the sensitive area, and the cell fires again shortly after the original pulse.

Cross-talk takes place when in a Geiger discharge, some of the electrons generated in the avalanche process reach the adjacent pixel, where another Geiger discharge might be triggered. This results in a pulse with a larger amplitude (nearly a factor two) and in a distortion of the linear response of the device.

Every detector can only convert a certain percentage of incident photons in signals. This G-APD efficiency is given as product of three factors:

$$\mathrm{PDE} = \mathrm{QE} \times \epsilon_{\mathrm{geom}} \times \epsilon_{\mathrm{Geiger}}, \tag{1}$$

where QE is the G-APD quantum efficiency, function of the incident photon wavelength, λ_{w}; ϵ_{geom} is a geometrical factor (fill factor) indicating which fraction of the device is sensitive to photons; $\epsilon_{\mathrm{Geiger}}$ is the probability to trigger a Geiger discharge and is function of $\mathrm{V_{bias}}$. PDE decreases with the pixel size.

Then, the G-APD response can be written as a product of few factors:

$$\mathrm{A} = \mathrm{N}_{\gamma}^{\mathrm{in}} \times \mathrm{PDE} \times \mathrm{g} \times (1 + \varepsilon) \times (1 + \mathrm{P_{AP}}), \tag{2}$$

where $\mathrm{N}_{\gamma}^{\mathrm{in}}$ is the number of incident photons; g, the gain; ε, the cross-talk probability and $\mathrm{P_{AP}}$, the after-pulse probability. It should be noticed that in the above equation, g, PDE, ε and $\mathrm{P_{AP}}$ are all increasing with $\mathrm{V_{bias}}$, implying a complex dependence of the G-APD response on the bias voltage.

3 Measurement setup

Figure 1 shows the scheme of the PDE measurements. The light from a Light-Emitting Diode (LED) operating in a pulse-mode with a Waveform Generator (AGILENT 33220A) was delivered to an optical filter. The latter corresponded to the peak wavelength of the LED and had a bandwidth of $\pm$ 3 nm. By changing the LED, a few wavelengths in the 380 $\div$ 650 nm range were investigated. For low intensity sources (380 nm, 400 nm, 565 nm) the LED light was not filtered.

The filtered light was routed to a light-tight thermostabilized box with inside two photodetectors: the G-APD and the reference photodetector. The box temperature was controlled at $\pm$ 0.1 °C during the data taking. As a reference photodetector a PhotoMultiplier Tube (PMT) H5783P produced and calibrated (for this reference) by HAMAMATSU was used. For each wavelength λ_{w} from the efficiency of the reference photodetector for the peak wavelength, as provided by the manufacturer, is derived the efficiency of the reference device, $\epsilon_{\mathrm{eval}}^{\mathrm{ref}}$, for our light source, taking in account the filter bandwidth or the LED full width half maximum.

The signal from G-APD is read out with a charge-sensitive preamplifier and digitized with an integrating ADC (CAEN QADC V792N). The LED pulse of about 6 ns duration and the ADC gate of about 65 ns width were synchronized by means of a common trigger. The integration time was long enough to contain most of G-APD signal. In case of the reference photodetector the direct signal from PMT was amplified with an external amplifier (NIM ORTEC 450) and digitized with the same ADC. Due to a high sensitivity to voltage variations, the G-APD

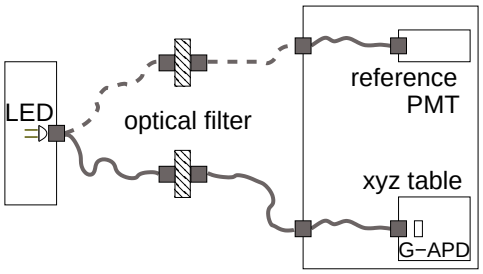

Figure 1: General scheme of the PDE measurements.

bias voltage was provided by a high precise
and stable in time voltage source (Keithley 6487/E).

4 Samples

The measurements refer to the samples listed in Tab. 1. The following operating conditions were chosen:

- HAMAMATSU produced Multi-Pixel Photon Counter S10362-11-025U [11] operated at $V_{bias} = 71.32$ V corresponding to $V_{over} \simeq 2.3$ V.
- CPTA produced SiliconPhotoMultiplier operated at $V_{bias} = 32.5$ and 32.7 V corresponding to $V_{over} \simeq 2.3$ V and 2.5 V. The parameter dependence on voltage has been studied in the range between 31.5 and 33.3 V.
- IRST produced SiliconPhotoMultiplier operated at $V_{bias} = 32$ V corresponding to $V_{over} \simeq 1.5$ V.

The temperature at data taking was T $\sim$ 23.7 °C stabilized at $\pm$ 0.1 °C during each measurement and with a spread $\pm$ 0.3 °C during all period of data taking.

Sample	Type	Photosensitive area [mm^2]	Number of pixels	Pixel pitch [μm^2]
HAMAMATSU	S10362-11-025U	1x1	1600	25x25
CPTA[1]	143	1.028[2]	556	43x43
IRST[3]	2007 prod	1x1	400	50x50

Table 1: Specification of measured samples. From left: Manufacturer, type, photosensitive area, number of pixels and their pitch. [1] Sample kindly provided by Prof. M. Danilov, [2] Sensitive area has octagonal shape, [3] Sample kindly provided by Dr. C. Piemonte (Fondazione Bruno Keller).

5 Measurement strategy and fit procedure

As described in Sec. 3 the PDE measurement strategy is based on the comparison of the effective number of photons detected from reference detector and G-APD.

To accomplish this task, noise and light (signal) response spectra of G-APD and PMT to a low number of photons have been measured and fitted, as described in the following.

The number of photons, n, detected per light pulse is expected to be Poisson distributed, with mean value λ. This distribution has to be convoluted with a gaussian distribution describing the experimental resolution. The charge x measured by the ADC is expected to have a frequency distribution, N(x):

$$\mathrm{N(x)} = \mathrm{N} \times \left(\mathrm{Poisson}(\lambda) \otimes \sum_{\mathrm{n}\geq 0} \mathrm{Gauss}(\mu_{\mathrm{n}}, \sigma_{\mathrm{n}}) \right),$$

or more explicitly:

$$\mathrm{N(x)} = \mathrm{N} \times \mathrm{e}^{-\lambda} \sum_{\mathrm{n}\geq 0} \left(\frac{\lambda^{\mathrm{n}}}{\mathrm{n!}} \times \frac{1}{\sigma_{\mathrm{n}}} \exp\left(\frac{-(\mathrm{x}-\mu_{\mathrm{n}})^2}{2\sigma_{\mathrm{n}}^2}\right) \right). \quad (3)$$

In the ideal case n photons correspond to a charge $\mu_{\mathrm{n}} = \mu_0 + \mathrm{n} \times \mathrm{g}$, where μ_0 is the pedestal position and g is the gain factor. In presence of a finite resolution the distribution of charge follows a gaussian distribution around each μ_{n} with a width σ_n, $\sigma_{\mathrm{n}}^2 = \sigma_0^2 + \mathrm{n} \times \sigma_1^2$, where σ_0 is the electronic noise (pedestal) width and σ_1 is the single photon width. N is a normalization factor.

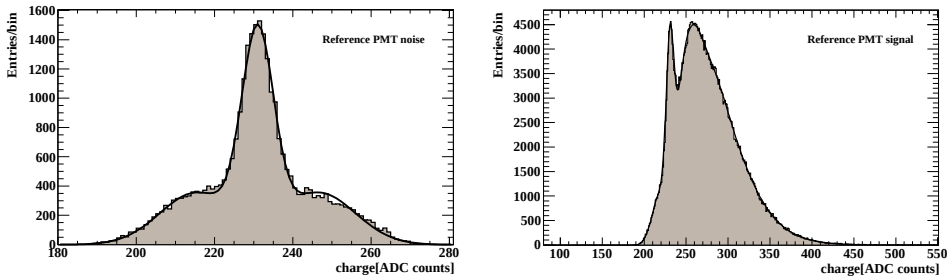

Figure 2: Reference PMT: noise (left) and signal (right) spectra. The signal is obtained by short, low-intensity LED flashes at $\lambda_{\mathrm{w}} = 450 \pm 3$ nm. The continuous lines are the fit results (see text). From the fit the mean number of detected photons is obtained, $\mathrm{N}_\gamma^{\mathrm{PMT}} = 1.71 \pm 0.02$ ($\epsilon_{\mathrm{eval}}^{\mathrm{ref}} = 20.33\ ^{+0.27}_{-0.28}\%$, see text). Binwidth=1.

Reference PMT fit procedure In the PMT case, it should be noticed that due to additional electrical noise caused by the external amplifier, the no-light spectrum (pedestal) is described as superposition of three gaussian peaks, two of which are considered to be symmetric. Figure 2 (left) shows the pedestal fitted with the sum of three gaussians. Figure 2 (right) shows the signal fitted with Eq. 3 modified to include the noise shape.

Using the mean number of detected photons, $\lambda = \mathrm{N}_\gamma^{\mathrm{PMT}}$, as obtained from the above fit, and the PMT efficiency, the mean number of photons delivered by the optical system to the photodetector surface per one LED pulse was estimated.

In the example of Fig. 2, at $\lambda_{\mathrm{w}} = 450$ nm, it is $\mathrm{N}_\gamma^{\mathrm{PMT}} = 1.71 \pm 0.02$. Taking into account the efficiency for this λ_{w}, $\epsilon_{\mathrm{eval}}^{\mathrm{ref}} = 20.33\ ^{+0.27}_{-0.28}$ %, the mean number of photons impacting PMT is obtained. This is the first step for the PDE calculation.

G-APD fit procedure Figure 3 shows typical G-APD HAMAMATSU response spectra, on the left for no light (noise) and on the right for low-intensity light (signal).

The noise spectrum shows beyond the first peak (pedestal) other peaks which are due to thermogeneration. Since their contribution to the total noise is about 2% of the pedestal, the thermogeneration effect can be neglected in the signal fit. Moreover since the probability of two or more thermogeneration counts within the gate is negligible, the cross-talk effect

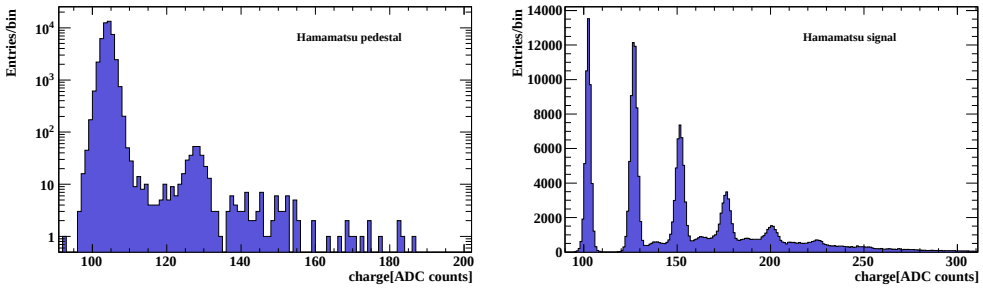

Figure 3: HAMAMATSU G-APD: noise (left) and signal (right) spectra. The signal is obtained by short, low-intensity LED flashes at $\lambda_w = 450 \pm 3$ nm. Each peak corresponds to a number of detected photons. Binwidth=1.

can be estimated from the ratio of the numbers of events in the 3^{rd} and 2^{nd} peak. This value ($\sim 20\%$) depends on the gate length (in our case 65 ns) and on the operation voltage, V_{bias} (Sec. 2).

In the signal spectrum the first peak (pedestal) corresponds to the noise, the second one is the G-APD response when exactly one photon is detected (one pixel is fired). It is impossible to identify which one of the pixels was fired, since they are all connected to the same output and they have similar responses. If n pixels are fired, the sum of n charges is recorded at the position of the $(n+1)^{th}$ peak, $\mu_n = \mu_0 + n \times g$.

These peaks, as shown in Fig. 3 (right), are equidistant, at a distance determined by the gain factor, g. The enhancements which show up between the peaks, were attributed to after-pulses (AP) and were considered in the fit.

To identify the most appropriate function describing this effect the main peaks, each fitted to a gaussian distribution, were subtracted from the spectrum of Fig. 3 (right). As a result, a sequence of peaks, Fig. 4 (left), was obtained, each one well described as a sum of two gaussians (for this G-APD and for the chosen gate length). This suggested to write a new fitting function P(x) as follows.

If P_n^0 is the probability to get initially n cells fired (the poissonian n term in Eq. 3), the probability to record an x charge, P(x)=N(x)/N can be written as sum of three terms representing respectively the probability of an x charge when n cells are fired 1) without AP, P_n^{noAP}; 2) when only one AP occurred, P_n^{AP1}; 3) when two APs occurred, P_n^{AP2}:

$$P(x) = \sum_n P_n^{noAP} \times Gauss(\mu_n, \sigma_n) + P_n^{AP1} \times Gauss(\mu_n + \delta_1, \sigma_1) + P_n^{AP2} \times Gauss(\mu_n + \delta_2, \sigma_2), \quad (4)$$

where $\delta_{1,2}$ are the distances of the first and second after-pulse gaussian from the nearest main peak and $\sigma_{1,2}$ the widths. The probabilities P_n^{noAP}, P_n^{AP1} and P_n^{AP2} are all functions of a single parameter P_{AP}, the probability to get an AP from one cell, and can be written as:

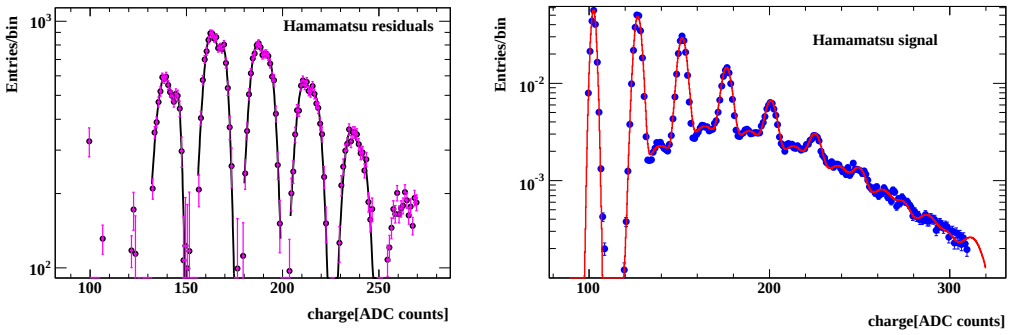

Figure 4: Residual distribution after subtraction of best-fitted gaussians from the signal spectrum (left). The signal spectrum fitted with the after-pulse corrections (right). From this fit, the probability, P_n^0, to get n cells fired and the probability, P_{AP}, to get an after-pulse from one cell are derived (in this example $P_{AP} = 0.16 \pm 0.01$). Binwidth=1.

$$
\begin{aligned}
P_n^{noAP} &= P_n^0 \times (1 - P_{AP})^n \ , \\
P_n^{AP1} &= P_n^0 \times (1 - (1 - P_{AP})^n) \times (1 - P_{AP})^n, \\
P_n^{AP2} &= P_n^0 \times (1 - (1 - P_{AP})^n) \times (1 - (1 - P_{AP})^n).
\end{aligned}
$$

If the probability of after-pulses is zero, the Eq. 4 is equivalent to Eq. 3.

Equation 4 was fitted to the spectrum of Fig. 3 (right) and the fit result is shown in Fig. 4 (right) as a continuous line. Among the free parameters, we obtain the P_n^0 values as displayed in Fig. 5 (black dots) and the after-pulse probability, $P_{AP} = 16\%$.

The P_n^0 values should be distributed according to the Poisson statistics with a mean number of photons detected, N_γ^{G-APD} (corresponding to the Poisson's distribution parameter λ). However this distribution is distorted by the presence of cross-talk. If the cross-talk probability is $\varepsilon \neq 0$, then the n=1 bin (2^{nd} peak in Fig. 4 (right)), contains only events with one initially fired cell without any cross-talk, with a probability $P(1) = P_1^0(1-\varepsilon)$. The n=2 bin ($3^{rd}$ peak) is filled either when two cells are initially fired without cross-talk or when one cell is fired accompanied by a second cell fired by cross-talk: $P(2) = P_2^0(1-\varepsilon)^2 + P_1^0\varepsilon(1-\varepsilon)$. Finally the probability to observe n fired cells P(n), can be written:

$$
P(n) = \sum_{j=1}^{n} P_j^0 (1-\varepsilon)^j \varepsilon^{n-j} \binom{n-1}{j-1}. \tag{5}
$$

The data in Fig. 5 (left) were fitted using Eq. 5; the red line represents the result of the fit. For these data, the value obtained for the cross-talk probability was $\varepsilon = 0.20 \pm 0.01$; the value of the mean number of detected photons is $N_\gamma^{G-APD} = 1.55 \pm 0.02$. In general, for any pair of measurements on G-APD sample, and on the reference PMT, we have:

$$
PDE = \frac{N_\gamma^{G-APD}}{N_\gamma^{PMT} \cdot \epsilon_{eval}^{ref}} \tag{6}
$$

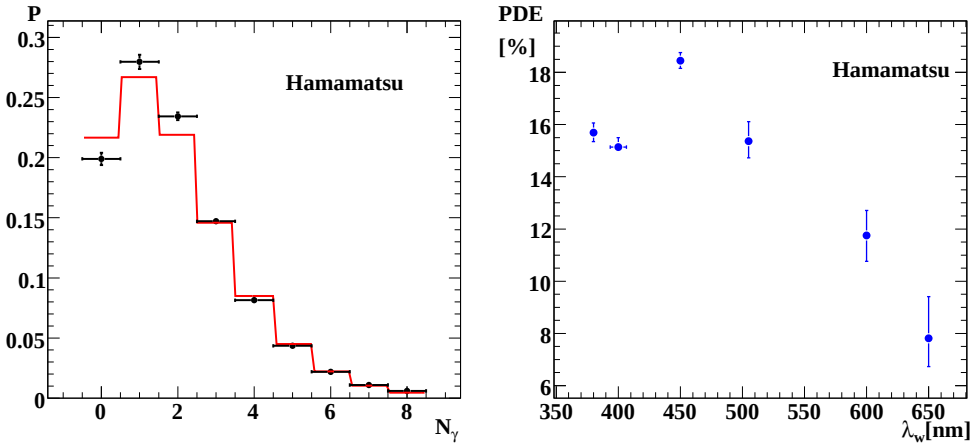

Figure 5: Right: distribution of probability, P, to observe N_γ photons. The data, black dots, are the P_n^0 obtained by fitting the signal spectrum (Fig. 4, right). The red line represents the fit of these data with Eq. 5. In this example, the fitted values are: the mean number of G-APD detected photons, $N_\gamma^{G-APD} = 1.55 \pm 0.02$, and the cross-talk probability, $\varepsilon = 0.20 \pm 0.01$. Binwidth=1. Left: The photon detection efficiency, PDE, for the HAMAMATSU G-APD as a function of the light wavelength, λ_w.

With the mean number of photons detected by G-APD, N_γ^{G-APD} and by PMT, the reference detector, N_γ^{PMT}, it is possible to evaluate the photon detection efficiency. In our example, the PDE value is 18.36 ± 0.26 % (statistical error only).

The final value of PDE is obtained as mean of various measurements at different light intensities, with different fiber configurations, taking into account the FWHM of the light source and the filter bandwidth.

The procedure and results described in this section for G-APD HAMAMATSU were as well applied to the others samples, with minor modifications. In the following sections these results are discussed.

6 Photon detection efficiency: Hamamatsu sample

Based on the fitting procedure of Sec. 5, it is possible to calculate for each measurement the corresponding PDE value. The measurements have been made at different light intensities and with different optical layouts to evaluate possible sources of systematics. The systematic error due to optical contact, excluding a statistical contribution, is $\sim 1\%$ in absolute value.

At this point, it is possible to evaluate the photon detection efficiency of the device as the mean of all available measurements. The results are shown in Fig. 5 (right). The horizontal error bar is originated from the light source FWHM or filter bandwith; its impact on PDE evaluation gives the vertical error bar.

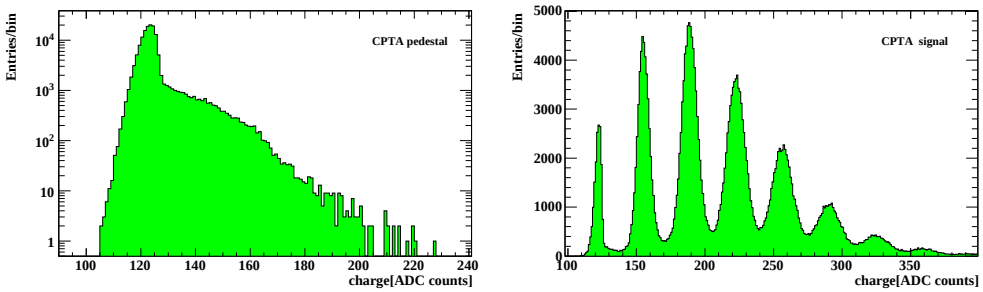

Figure 6: The noise (left) and signal (right) spectra obtained with the CPTA G-APD illuminated by short, low intensity LED flashes at $\lambda_w = 600 \pm 3$ nm. Each peak corresponds to a number of detected photons. Binwidth=1.

7 Photon detection efficiency: CPTA sample

The noise and the signal spectra obtained with the CPTA sample, as shown in Fig. 6 for $\lambda_w = 600 \pm 3$ nm, reflect the difference on the construction characteristics. With respect to the HAMAMATSU device Fig. 6 (left) shows that with the chosen gate the thermogeneration is at a level of $\sim 30\%$, and Fig. 6 (right) shows that the after-pulses have lower impact on the single photon spectra. The cross-talk effect is much lower. The fit procedure adopted for the CPTA device is slightly different from that described in Sec. 5. The thermogeneration contribution was not included in the fit, the AP terms (Eq. 4) were not directly related to an after-pulse effect but accounted also for the termogeneration and other effects.

The PDE results for other wavelengths are shown in Fig. 7 (left). The horizontal error bar is originated from the light source FWHM or filter bandwidth, the vertical one from its impact on the PDE evaluation. The measurements have been recorded at V_{bias}=32.5 V for λ_w= 450 nm, 565 nm, 600 nm and V_{bias}=32.7 V for λ_w= 500 nm and 600 nm. The measurement at λ_w= 600 nm has been recorded at both voltages.

7.1 Parameter dependence on overvoltage: PDE

The photon detection efficiency, PDE_{rel}, relative to the one at the reference voltage as a function of V_{bias} has been recorded at different wavelengths. From a straight line fits ($PDE_{rel} = p_0 + p_1 V_{bias}$) these distributions the values for the angular coefficients, $p_1[V^{-1}]$ are derived and the PDE value as a function of λ_w at various values of V_{bias} is obtained, Fig. 7 (right) . The validity of the method is tested with the measurements at 600 nm, taken at two different bias voltages.

7.2 An improved fit procedure

The CPTA G-APD measurements described above have two peculiar aspects that deserve more attention: the thermogeneration effect is not negligible (Fig. 6 (left) and the after-pulse effect requests a dedicated treatment. We refere to [10], for a detailed description of the method.

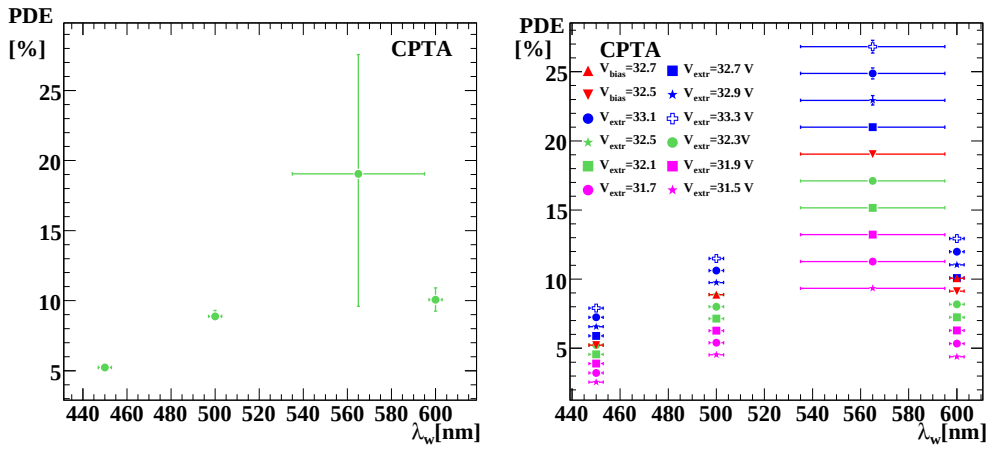

Figure 7: Left: the photon detection efficiency, PDE, for CPTA G-APD as a function of the light wavelength, λ_w. The measurements at 450 nm, 565 nm, 600 nm have been recorded at V_{bias}=32.5 V, those at 500 nm, 600 nm at V_{bias} = 32.7 V. The λ_w = 600 nm measurements at the two bias voltages are indistinguishable. Right: the photon detection efficiency, PDE, for the CPTA detector as a function of the wavelength, λ_w, as measured (red points) and extrapolated (green, blue, magenta points).

As a first step the termogeneration spectrum shape is determined as a deviation of the noise spectrum, Fig. 6 (left), from a gaussian. A combination of two exponential functions results into an appropriate description of this effect.

As second step the fit of the signal pedestal is not performed with a simple gaussian as above, but includes also the fit function determined in the first step and describing the termogeneration.

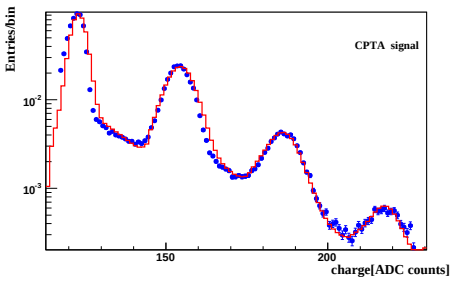

Figure 8: The CPTA G-APD signal spectrum (at λ_w=450 ± 3 nm) fitted with the improved fit procedure, Sec. 7.2.

Further improvement in the signal fit is achieved, if the after-pulse effect is modeled for a single fired pixel, as suggested in Sec. 2. The results of this improved method are shown in Fig. 8.

Using this fit procedure it is possible to derive a value of the cross-talk probability and the average obtained on measurements performed at many light intensities is $\leq 1.7\%$.

Similar measurements were recorded with a IRST device. Again, the noise and signal spectra reflect the difference on construction and design. From these spectra we have concluded that the specimen used wasn't suitable for PDE measurements.

8 Conclusion

Measurements of G-APD response to low intensity light were recorded to determine the main characteristics of three different samples, HAMAMATSU (S10362-11-025U), CPTA, IRST. An accurate method to fit the response has been realized, to evaluate photon detection efficiency, cross-talk, gain, and after-pulse probability. A calibrated reference detector has been used for the photon detection efficiency measurements in a wavelength range between 380 and 650 nm, see Ref. [10].

The measurements were carried on in the same experimental condition (setup, thermal insulation...) to compare the properties of various samples. This information is an important issue in the near future to identify the most suitable device for a particular application in high-energy physics calorimeters, astroparticle physics and medical environment.

The PDE measurements provided are consistent with those quoted from the manufacturers with a *caveat* due to the different method of measurement (the current method, very often used by manufacturers, includes after-pulse and cross-talk effects).

9 Acknowledgments

We would like to thank Profs. M. Danilov and E. Tarkovsky for the samples provided and clarifying discussions, Dr. I. Polak for having provided a fundamental part of electronics, and Prof. Maria Fidecaro for comments to the manuscript.

10 Bibliography

References

[1] G. Bondarenko G. *et al.*, Nucl. Phys. Proc. Suppl. **61B** 347 (1998).

[2] P. Buzhan *et al.*, Nucl. Instrum. Meth.A **504** 48 (2003).

[3] V. Golovin and V. Saveliev, Nucl. Instrum. Meth.A **518** 560 (2004).

[4] B. Dolgoshein *et al.*, Nucl. Instrum. Meth.A **563** 368 (2006).

[5] K. Yamamoto *et al.*, IEEE Nucl. Sci. Symp. Conf. Rec. **2** 1094 (2006).

[6] N. Dinu *et al.*, Nucl. Instrum. Meth.A **572** 422 (2007).

[7] G. Bonanno *et al.*, Nucl. Instrum. Meth.A **610** 93 (2009).

[8] M. Danilov, Nucl. Instrum. Meth.A **604** 183 (2009).

[9] M. Danilov, Nucl. Instrum. Meth.A **581** 451 (2007).

[10] S. Gentile, E. Kuznetsova and F. Meddi submitted for publication to Nuovo Cimento B.

[11] HAMAMATSU PHOTONICS K.K., Product catalogue No. KAPD0002E02 (2007).

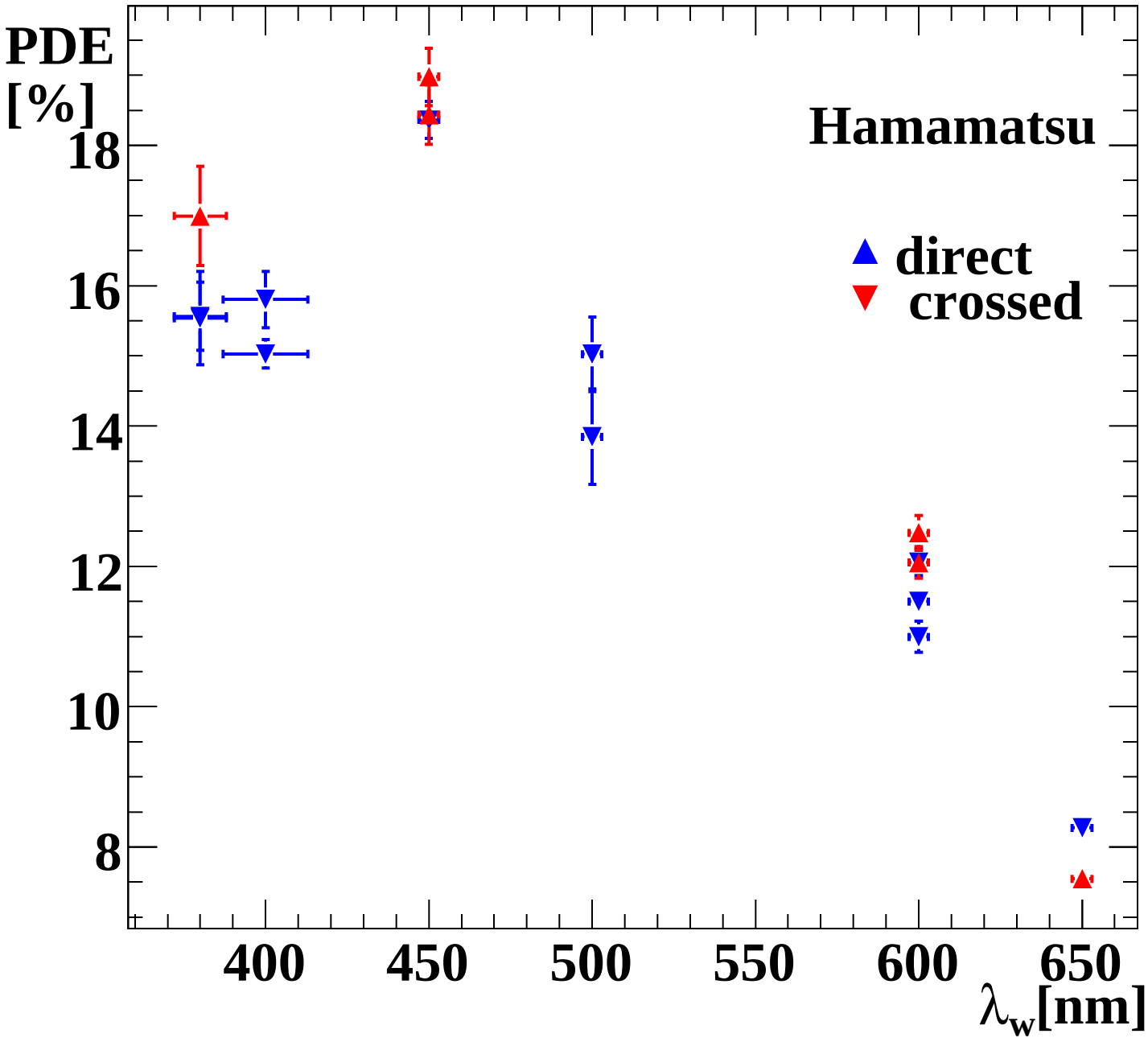
PDE
[%]
18
16
14
12
10
8
400
450
500
550
600
650
λw[nm]
Hamamatsu
direct
crossed